Professor Emeritus Don McGlinchey

CFD Mesh Convergence & CFD–DEM Modeling for Pneumatic Conveying

mesh generation, y^+ wall resolution, Richardson Extrapolation (GCI), and length-scale conflicts in continuum-discrete solvers, etc.

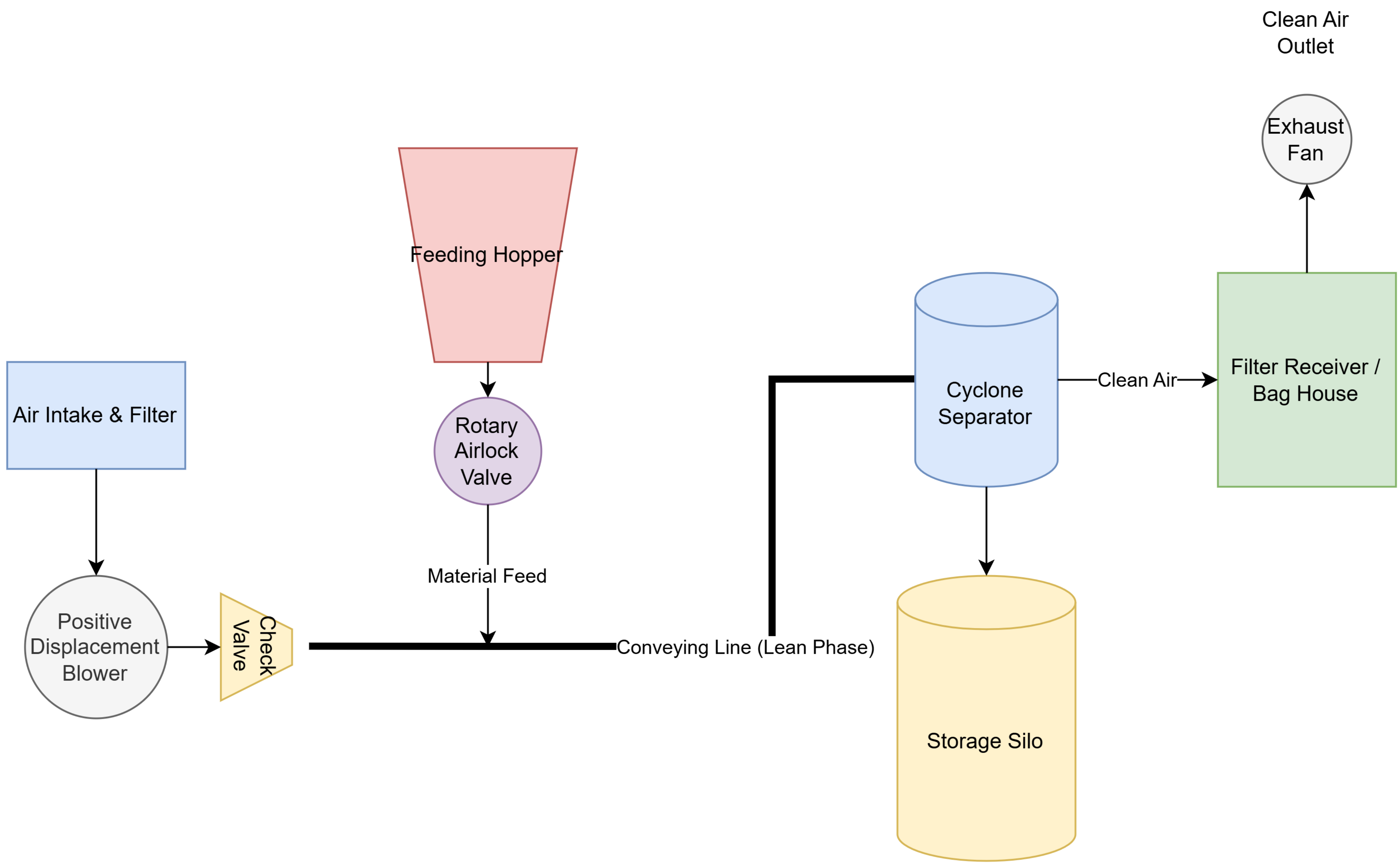
Clean Air
Outlet
Exhaust
Fan
Feeding Hopper
Cyclone
Separator
Clean Air
Filter Receiver /
Bag House
Air Intake & Filter
Rotary
Airlock
Valve
Material Feed
Positive
Displacement
Blower
Check
Valve
Conveying Line (Lean Phase)
Storage Silo

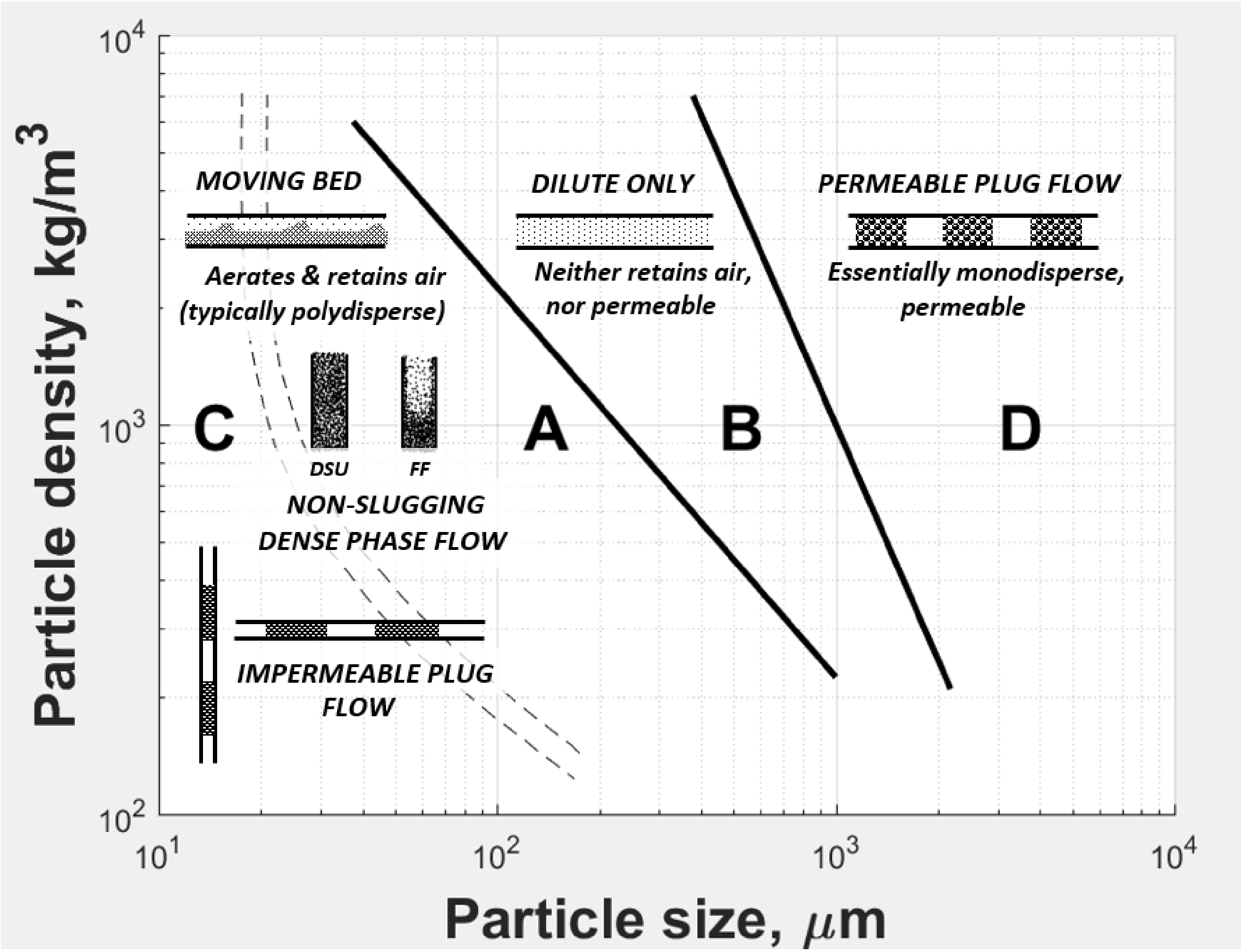

Phase Maps for Fluidized Dense Phase Conveying and Validation by Eulerian Modelling
Balasubramanian, P. (Author). 2025
GCU: Doctoral Thesis › Doctor of Philosophy (PhD)

Flow Characterisation & Near-Wall Setup

Dilute Phase: Flow Regime & Turbulence Modeling: With Pipe Diameter D = 0.1 m, Velocity U = 20 m/s, and kinematic viscosity $\nu \approx 1.5 \times 10^{-5}$ m²/s, the Reynolds Number is $Re = UD/\nu \approx 1.33 \times 10^5$ (comfortably turbulent). This suggests a RANS k-ω SST turbulence model for internal wall-bounded flows.

Inlet Boundary Condition: Developing full turbulent flow naturally requires entrance length

$$\frac{L_e}{D} \approx 4.4 Re^{\left(\frac{1}{6}\right)} \approx 31D(\ 3.1m).$$

To save compute, prescribe a fully developed power law turbulent profile directly at the inlet.

Flow Characterisation & Near-Wall Setup

Viscous Sublayer Resolution ($y^+ \approx 1$): Using Blasius shear stress estimation ($\tau_w \approx 0.99\ Pa, u_\tau \approx 0.91 \frac{m}{s}$), resolving $y^+ \approx 1$ for SST requires a first cell height

$$\Delta y = \frac{y^+ \nu}{u_\tau} \approx 16.5\ \mu m.$$

Wall Functions ($y^+ = 30–100$): Acceptable for bulk pressure drop alone, requiring $\Delta y \approx 0.5 - 1.65\ mm$. However, in a 50 mm radius pipe, high y^+ cells occupy a non-trivial radial fraction.

See; https://en.wikipedia.org/wiki/Law_of_the_wall

Mesh Topology & Boundary Layer Layering

Cross-Sectional Topology

Avoid Polar O-Grids: Standard polar grids create single central singularities with highly skewed triangular/wedge elements on the pipe axis.

Butterfly Block Topology: Implements an O-grid inside a central square core block. Generates 100% all-hexahedral cells, preserves high orthogonal quality, and ensures high gradient accuracy across the entire cross-section.

Layering & Resolution Limits

Inflation Stack: Construct 20–25 prism/hex inflation layers from the pipe wall with a growth rate of 1.15–1.20 to transition smoothly to the core mesh.

Axial Aspect Ratios: Axial cell size can be coarser than radial, but keep boundary layer cell aspect ratios broadly under 20–50:1 to maintain solver convergence stability.

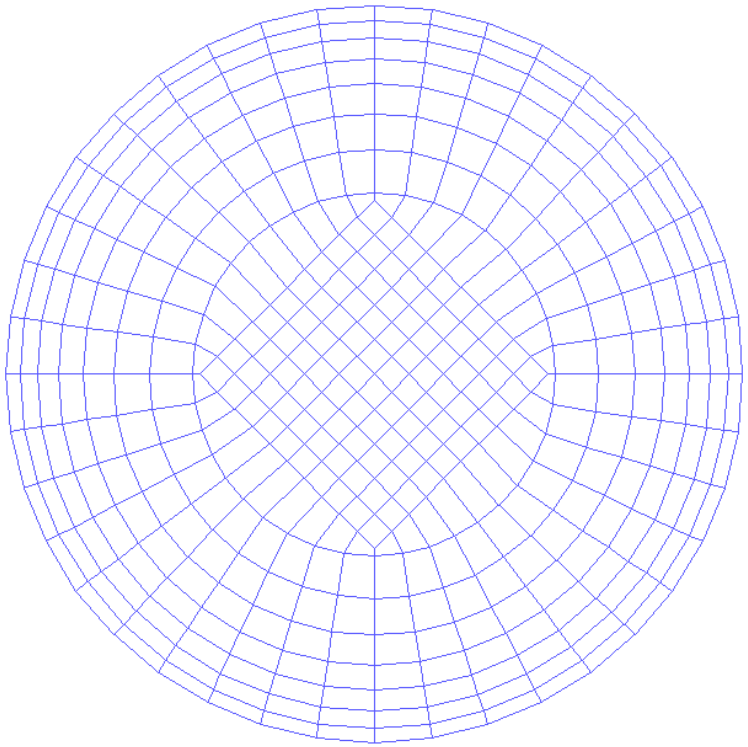

“Butterfly” Block Topology

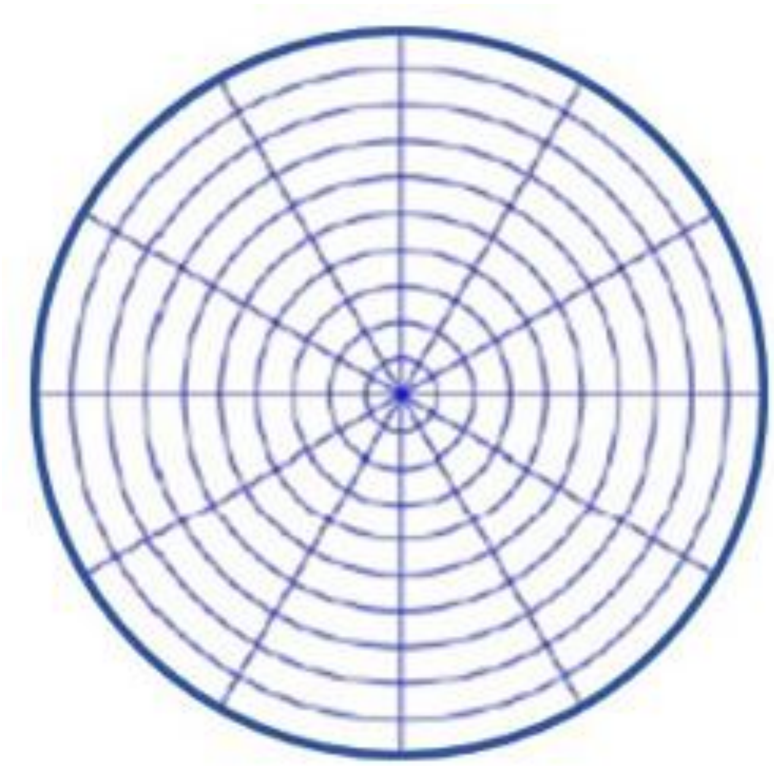

Polar O-Grid

Overview of the V&V-20 Validation Procedure

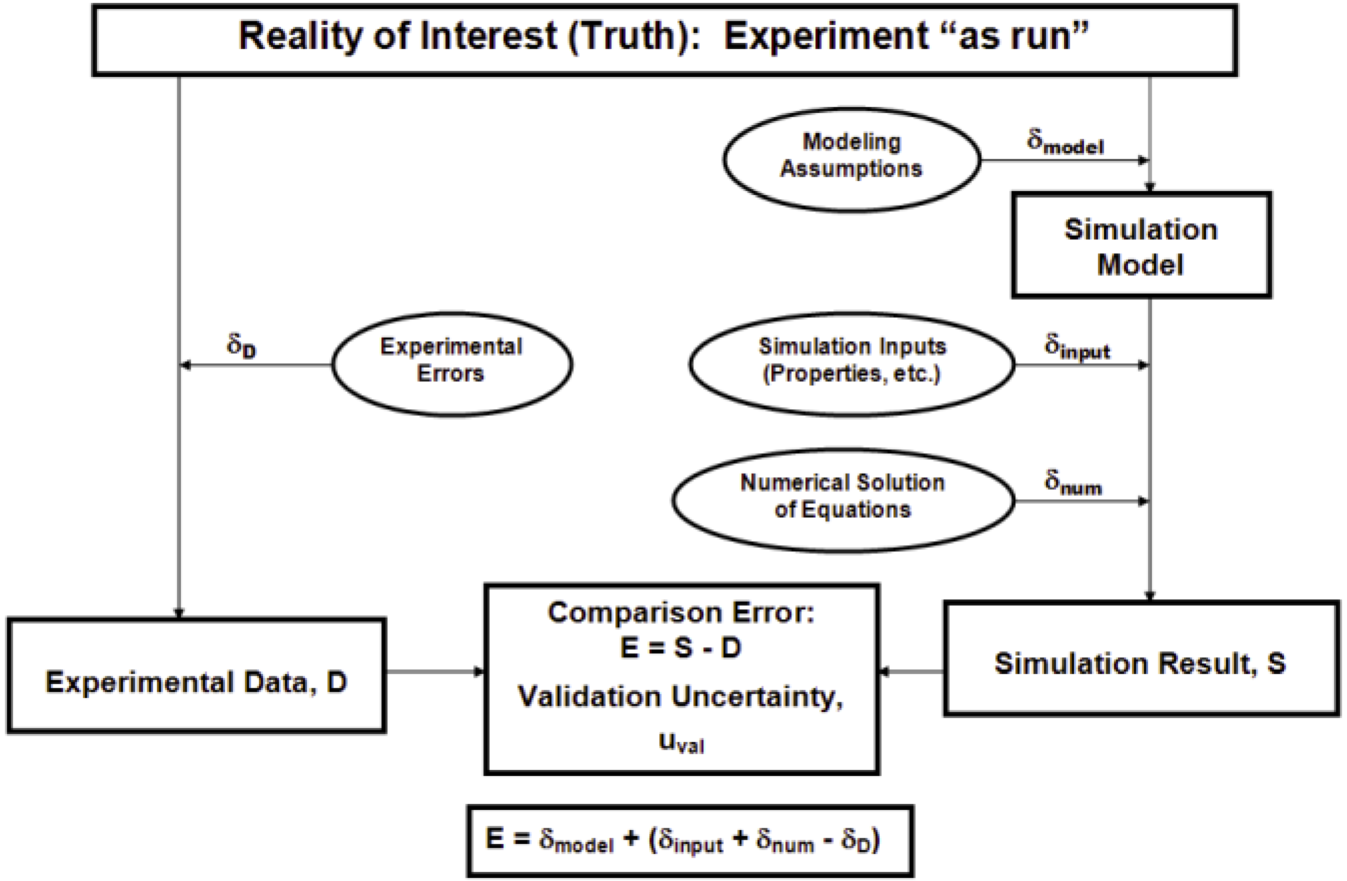

https://www.osti.gov/servlets/purl/1368927

Verification & GCI Rigor (ASME V&V 20)

3-Mesh Requirement

Use at least 3 uniformly refined meshes (Coarse, Medium, Fine) with constant refinement ratio

$$r = \frac{h_{coarse}}{h_{fine}} \geq 1.3 \left(e.g. r = \sqrt{2}\right).$$

Cell count scales as r^3 (~2.83×).

Observed Order (p)

Compute formal order of convergence from key scalar (f or ΔP):

```
p = ln[(f₃ - f₂)/(f₂ - f₁)] /
ln(r)
```

Verify p matches theoretical scheme order (~2.0).

Fine-Grid GCI Band

Calculate discretisation uncertainty using safety factor $F_s = 1.25$:

```
GCI_fine = (F_s · |ε|) / (rᵖ -
1)
```

Target GCI < 1–2% for integral pressure drop or wall shear.

Case Study: 4-Mesh Convergence Data

Mesh Level	Cell Count	First Cell Δy	Achieved y^+	Friction Factor (f)	Rel. Error ε (%)	Order (p)	GCI_fine (%)
M1 (Coarse)	0.90 M	33.0 µm	1.5 – 2.3	0.01750	—	—	—
M2 (Medium)	2.55 M	23.3 µm	1.1 – 1.6	0.01705	2.57%	—	—
M3 (Fine)	7.20 M	16.5 µm	0.8 – 1.1	0.01682	1.35%	1.94	1.79%
M4 (Finest)	20.4 M	11.7 µm	0.6 – 0.8	0.01671	0.65%	2.13	0.75%

* Extrapolated benchmark f_ext ≈ 0.01681 (M2-M3-M4 triplet). Refinement ratio r = √2 (1.414). Asymptotic ratio check GCI_M3 / (r^p · GCI_M4) ≈ 1.01 confirms asymptotic convergence.

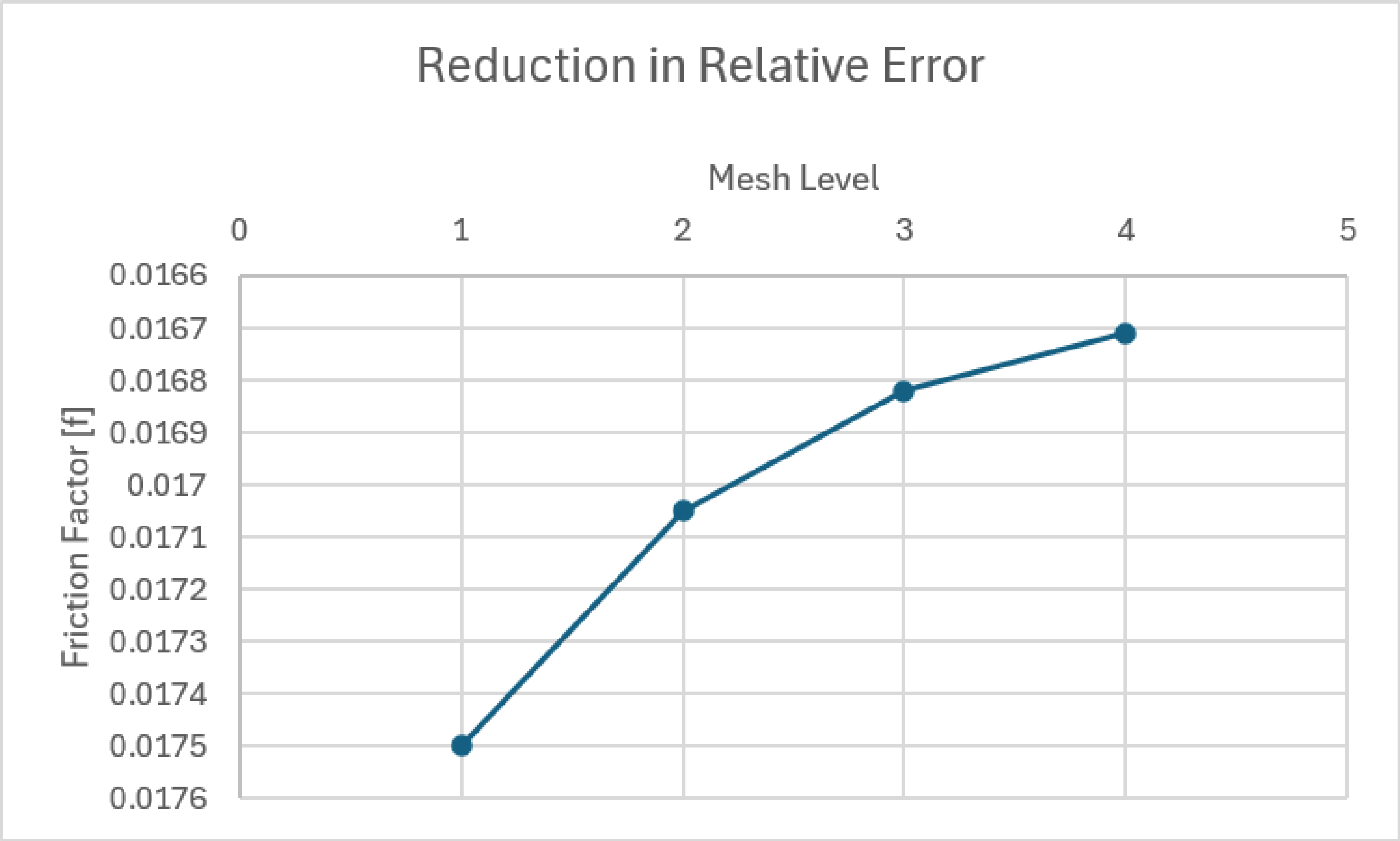

Reduction in Relative Error
Mesh Level
0
1
2
3
4
5
Friction Factor [f]
0.0166
0.0167
0.0168
0.0169
0.017
0.0171
0.0172
0.0173
0.0174
0.0175
0.0176

Scale Conflict: Unresolved CFD-DEM Coupling

The Core Physical Constraint

Unresolved Point-Particle Assumption: Fluid voidage (ε_f) in a cell is computed from particle centroids inside it. Statistically smooth fields require cells to hold a sufficient particle population.

Unphysical Voidage Jumps: If cell size $\Delta x < 3\ d_p$ (e.g. < 6 mm), particles crossing faces cause abrupt jumps in voidage, leading to noisy drag force source terms and solver instability.

Direct Conflict with $y^+ \approx 1$: A single-phase $y^+ \approx 1$ first layer (16.5 µm) is ~100 times smaller than d_p (2 mm). Continuum volume-averaging completely breaks down near the wall!

CFD–DEM Mesh & Wall Boundary Strategy

Wall Function Transition

Abandon Sublayer Resolution: Low-Re $y^+ \approx 1$ meshes are physically invalid in point-particle CFD-DEM.

Switch to wall functions with first cell height dictated by the particle floor $\Delta y \geq 3d_p$ ($\geq$ 6 mm).

Check Resulting y^+: Evaluate whether y^+ lands within the 30–100 log-law window. Flag any conflict between DEM cell size limits and wall function validity.

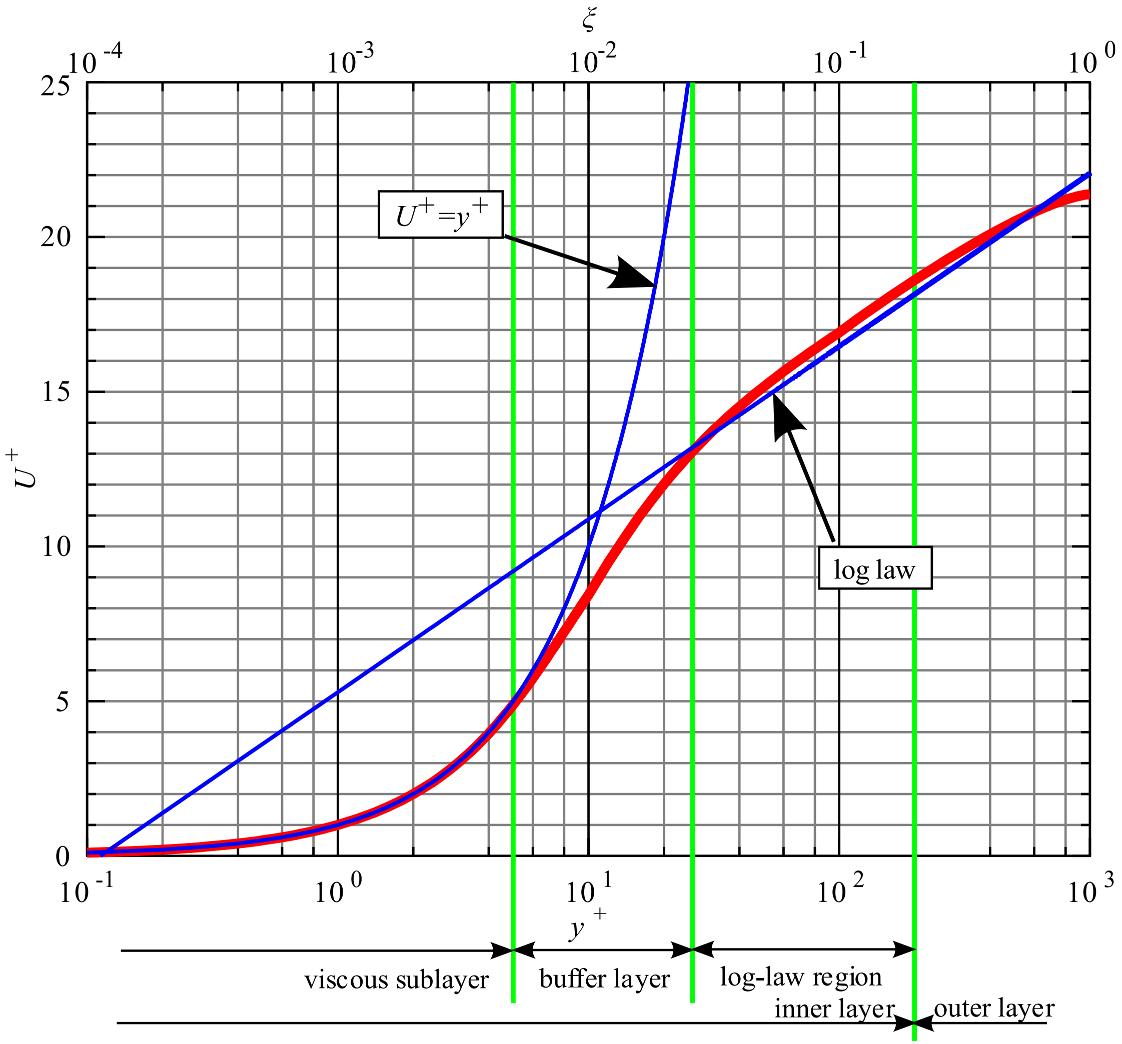
ξ
10 -4
10-3
10-2
10 -1
10 0
25
20
15
10
5
0
U+
U+=y+
log law
10 -1
10 0
10 1
10 2
10 3
y+
viscous sublayer
buffer layer
log-law region
inner layer
outer layer

CFD-DEM Mesh & Wall Boundary Strategy

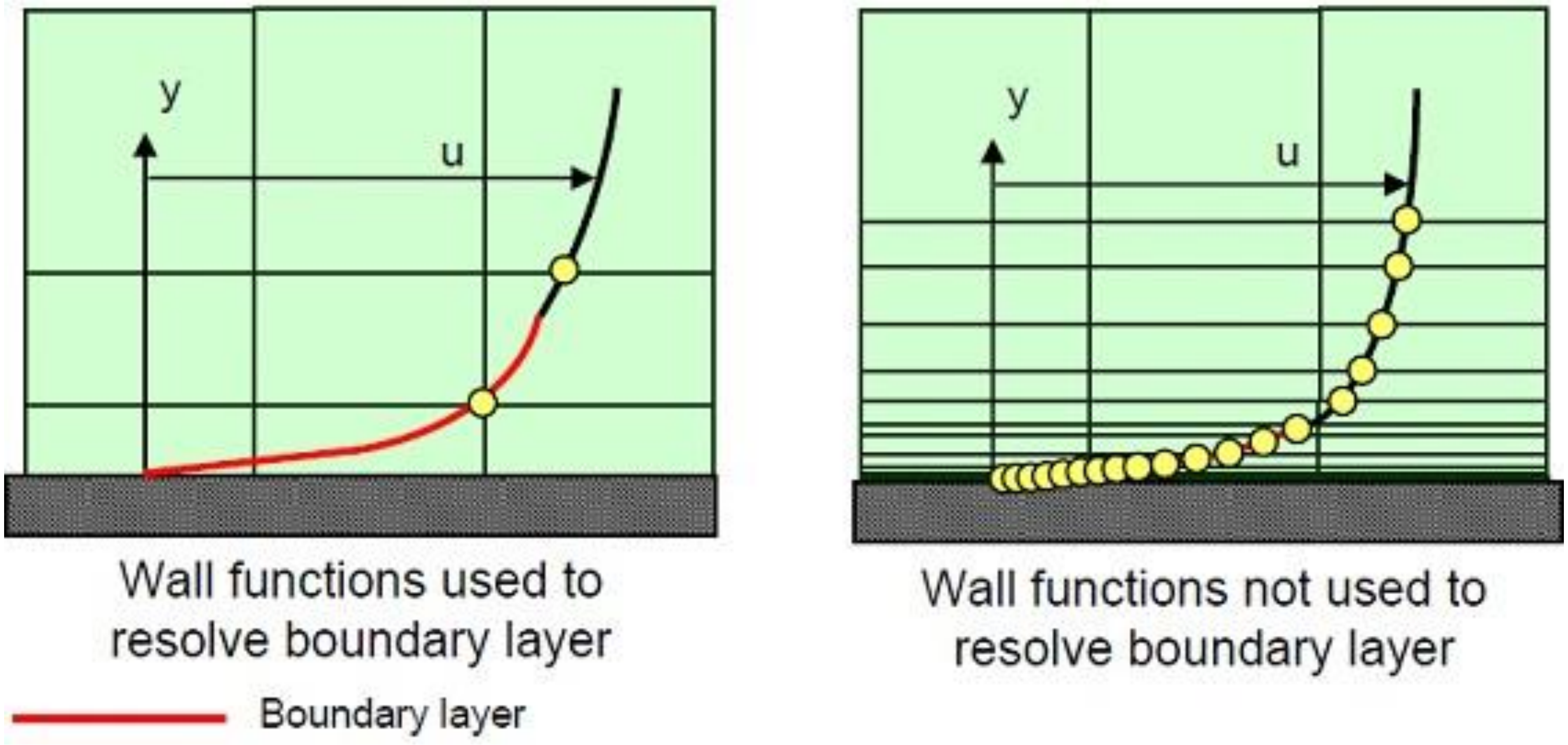

https://www.leapaust.com.au/blog/cfd/tips-tricks-inflation-layer-meshing-in-ansys/

CFD-DEM Mesh & Wall Boundary Strategy

Core Mesh & Boundary Layer

Reduced Inflation Stack: Reduce inflation stack to 4–6 layers with coarser growth rates to transition smoothly from the 6 mm wall cell to core cells.

Core Cell Size Trade-Off: Coarsen core cells to 6–10 mm. In a 100 mm pipe, 10 mm cells provide only 10 cells across diameter—hold near $3d_p$ (6 mm, ~16 cells) to balance drag stability with flow resolution.

Parameter Comparison: Single-Phase vs Unresolved CFD-DEM

Parameter	Single-Phase Resolved (Fluid)	Unresolved CFD-DEM (d_p = 2 mm)
Governing Constraint	Near-wall turbulence scale ($y^+ \approx 1$)	Voidage statistical smoothness ($\Delta x / d_p \geq 3$)
First Cell Height (Δy)	~16.5 µm (Viscous Sublayer resolved)	≥ 6.0 mm (3 d_p particle floor limit)
Turbulence Model	k-ω SST (No wall functions)	Standard Wall Functions (y^+ subordinate to d_p)
Boundary Inflation	20–25 layers, growth 1.15–1.20	4–6 layers, coarse growth rate
Core Cell Size	2.0 – 3.0 mm	6.0 – 10.0 mm
Pipe Cross-Resolution	High resolution across 100 mm diameter	~10 to 16 cells across 100 mm diameter

Coarse-Graining Voidage Kernels

Particle Centroid Method

Standard PCM: Binary cell assignment based on particle center. Highly mesh-sensitive; fails when $\Delta x < 3 d_p$ due to step-change voidage fluctuations.

Divided Particle Volume

DPVM: Distributes sphere volume across intersecting mesh cell faces. Smooths local voidage but remains bounded by particle size scale.

Diffusion Method

Transient Diffusion Kernel: Solves a continuous diffusion equation to filter voidage and drag forces. Decouples mesh size from d_p, enabling sub-particle cell refinement (Sun & Xiao, 2015).

Coarse-Graining Voidage Kernels

Particle Centroid Method

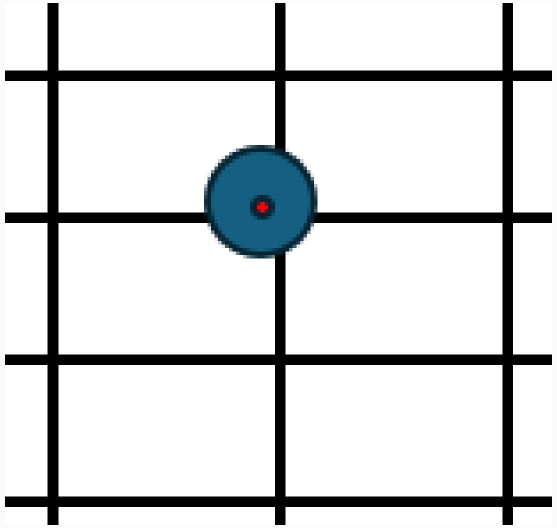

Divided Particle Volume

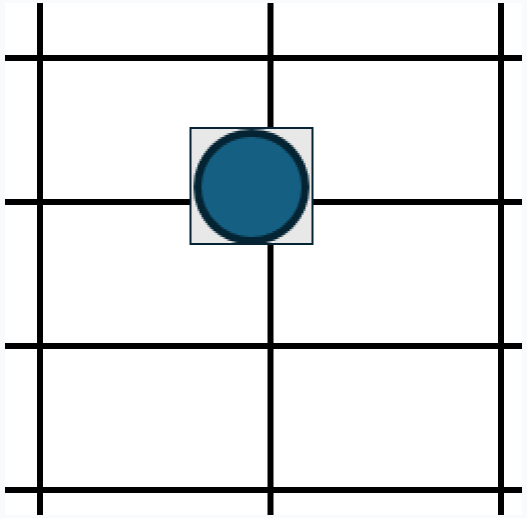

Diffusion Method

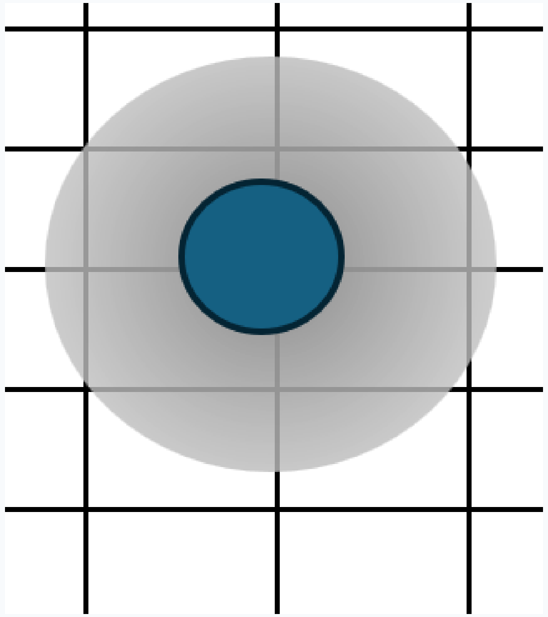

Multiphase Resolution Spectrum

Unresolved & Hybrid Regimes

Unresolved CFD-DEM: Uses Reynolds-Averaged Navier-Stokes (RANS) with empirical drag closures $(\Delta x \geq 3\, d_p)$. Scales to 10^7 particles.

Semi-Resolved Hybrids: Kernel-based reconstruction and two-grid formulations bridge local gradient accuracy with macro-scale efficiency.

Fully-Resolved Regime

Particle-Resolved DNS (PR-DNS): Directly resolves boundary-layer fluid mechanics and surface stresses, $\frac{d_p}{8}$ to $\frac{d_p}{50}$ grid spacing.

Particle Number Ceiling: Highly accurate micro-physics limited to $10^2 - 10^3$ particles due to supercomputing bottlenecks.

Particle-Resolved DNS Mechanics

Direct Interface Resolution: Implements no-slip boundary conditions directly on the particle surface using Lattice Boltzmann Moving-Explicit-Interface (LBM-MEM), Immersed Boundary (IBM), or boundary-fitted grids.

Stress Surface Integration: Hydrodynamic forces (drag, lift, torque) are evaluated by directly integrating local fluid pressure and viscous stress tensors over every particle's geometry.

Four-Way Physical Coupling: Captures particle-particle and particle-wall collisions via DEM (Hertzian, soft-sphere, linear spring-dashpot models, etc.) alongside short-range lubrication hydrodynamics.

PR-DNS Limits & Applications

$\frac{d_p}{50}$ Max Grid Spacing Req. Spacing < 10^{-3}d required for short-range lubrication

Computational Demands & Domains

Prohibitive Compute Cost: Requires massively parallel MPI/GPU execution on supercomputers, running for weeks for modest particle numbers $O(10^2)$– $O(10^3)$.

Primary Application Domains: Fundamental turbulent flow physics, pore-scale modeling, cake filtration, and derivation of constitutive drag laws.

The Immersed Boundary Method

The **Immersed Boundary Method (IBM)** is a numerical technique that models fluid-structure interactions by solving the fluid equations on a simple, fixed grid (Eulerian frame) while representing complex or moving boundaries using independent surface marker points (Lagrangian frame).

Lagrangian-Eulerian Coupling: Boundary forces are calculated at discrete surface points and distributed to surrounding background grid nodes using kernel functions (such as regularized Dirac delta functions) or ghost-cell interpolations.

Velocity Interpolation: The fluid velocity at Lagrangian markers is interpolated from neighbouring Eulerian grid nodes to enforce no-slip conditions $(\mathbf{u}_{\text{fluid}} = \mathbf{u}_{\text{solid}})$.

Lubrication Forces: When two particles collide, fluid is squeezed out between them. Because the fluid grid cannot resolve sub-grid gaps, an explicit sub-grid lubrication force model must be added before DEM contact occurs.

The Immersed Boundary Method

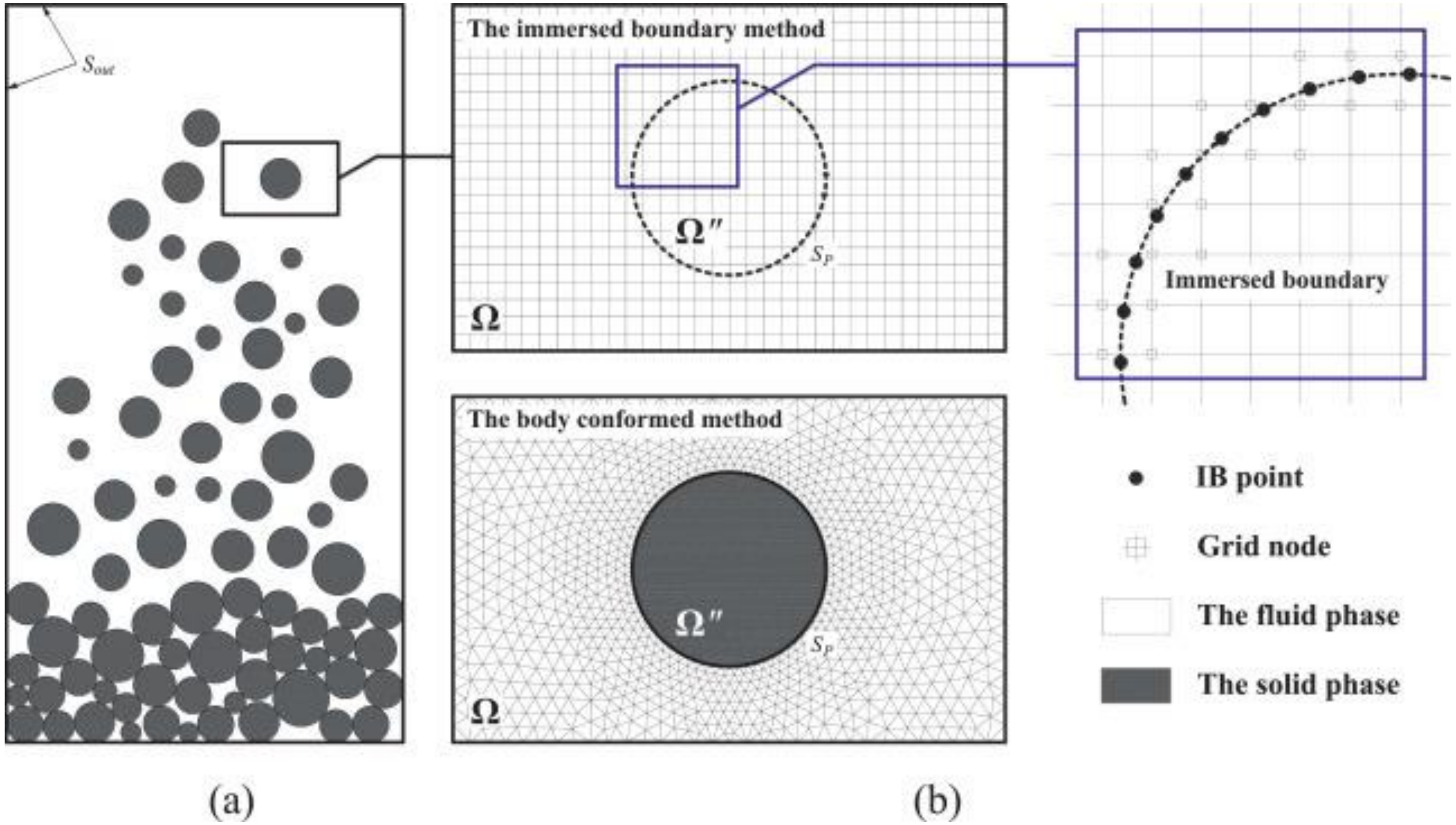

Yingtang Di, Lanhao Zhao, Jia Mao,A resolved CFD-DEM method based on the IBM for sedimentation of dense fluid-particle flows, Computers & Fluids, Volume 226, 2021, https://doi.org/10.1016/j.compfluid.2021.104968.

Two-Grid Multiphase Method

Independent Mesh Topologies

Fine CFD Mesh: Refined locally to resolve steep fluid gradients, shear layers, and complex boundary geometries.

Coarse DEM Mesh: Coarsened to maintain grid cell sizes $> 3\, d_p$ for smooth void fraction and drag force averaging.

Inter-Grid Mapping & Performance

Spatial Mapping: Solid fractions and momentum exchange are calculated on coarse DEM cells and mapped to fine CFD cells via interpolation.

Performance Balance: Adds minor communication overhead but drastically reduces memory and improves parallel scalability for large systems.

Method Comparison Matrix

Methodology	Grid Constraint	Coupling Mechanism	Max Particles	Primary Application Domain
PR-DNS (Fully Resolved)	$\Delta x \sim \frac{d_p}{8} to \frac{d_p}{50}$	Direct surface stress integration	$O(10^2)$ – $O(10^3)$	Fundamental turbulence, drag correlation derivation
Unresolved CFD-DEM	$\Delta x \approx 3 to 6 d_p$	RANS + Empirical Closures (Drag models)	$O(10^5)$– $O(10^7)$	Industrial fluidized beds, pneumatic conveying
Semi-Resolved (Kernel)	$\frac{\Delta x}{d_p} \approx 0.3 to 3.0$	Gaussian weighting kernel reconstruction	Moderate $O(10^4)$	Additive manufacturing, porous media flows
Semi-Resolved (Two-Grid)	CFD fine; DEM $>$ $3 d_p$	Coarse interaction mapping to fine fluid	High $O(10^6)$	Complex geometry industrial equipment analysis

Typical Method Use Cases

PR-DNS: micro-scale physics, pore-scale filtration, or calibrating new interphase drag closures for non-spherical particles.

Kernel / Two Grid / IBM: local fluid velocity/temperature gradients are critical but particle counts exceed PR-DNS limits (e.g. laser powder bed fusion).

Unresolved CFD-DEM: full-scale industrial plant equipment modeling ($10^5 to 10^7$ particles) where empirical closures provide sufficient bulk accuracy.

applied sciences

an Open Access Journal by MDPI

- International, peer-reviewed, open access journal focused on all aspects of applied natural sciences, published semimonthly online

- Editor-in-Chief: Prof. Dr. Giulio Nicola Cerullo, Dipartimento di Fisica, Politecnico di Milano, Milano, Italy

- High Visibility: indexed within Scopus, SCIE (Web of Science), Ei Compendex, Inspec, CAPlus / SciFinder, and other databases.
    - Impact Factor: 2.9
      Q2: Engineering, Multidisciplinary
    - CiteScore: 6.1
      Q1: General Engineering
      Q1: Instrumentation
      Q1: Fluid Flow and Transfer Processes
      Q2: Computer Science Applications
      Q2: General Materials Science
      Q2: Process Chemistry and Technology

- Journal Awards: Young Investigator Award
  Travel Award
  Best PhD Thesis Award
  Outstanding Reviewer Award
  Best Paper Award

2011	Journal was founded
40	Days submission to publication
119,908,301	Article views in 2025
58%	Rejection rate in 2025

E-Mail: applsci@mdpi.com

X: @applsci

LinkedIn: @Applied Sciences MDPI

applied sciences
an Open Access Journal by MDPI

IMPACT FACTOR 2.9
CITESCORE 6.1

Special Issue: Simulation and Measurement of Multiphase Flows in Industrial Applications

The special issue is coming soon.

Guest Editors:

Prof. Dr. Don McGlinchey
Glasgow Caledonian University, UK

Dr. Seyedahmad Hosseini
Glasgow Caledonian University, UK

Multiphase flows play a central role in a wide range of industrial applications, including energy systems, chemical and process engineering, pharmaceuticals, food production, and environmental technologies. The accurate prediction and measurement of such flows remains challenging due to their inherent complexity, involving strong phase interactions, turbulence, interfacial dynamics, heat and mass transfer, and phase change.

Recent advances in numerical simulation techniques—such as DNS, LES, advanced Eulerian and Lagrangian approaches, and the use of ML and AI—along with progress in experimental and non-intrusive measurement methods, have significantly improved our ability to study multiphase flows under industrially relevant conditions. However, challenges persist in model validation, scale-up, and the integration of simulations with experimental data.

This Special Issue aims to present recent developments in the simulation and measurement of multiphase flows, with a strong focus on industrial applications and the synergy between modelling and experiments. Original research articles and reviews are welcome.

Math. Model. Nat. Phenom.
Vol. 6, No. 3, 2011, pp. 2-27
DOI: 10.1051/mmnp/20116301

Observations Regarding Algorithms Required for Robust CFD Codes

F. T. Johnson [1]*, D. S. Kamenetskiy[2], R. G. Melvin[2], V. Venkatakrishnan[2], L. B. Wigton[2], D. P. Young[2], S. R. Allmaras[2], J. E. Bussoletti[2] and C. L. Hilmes[2]

[1] Contractor to The Boeing Company through YourEncore
[2] The Boeing Company, PO Box 3707, Seattle, Washington 98124-2207, USA

Abstract. Over the last three decades Computational Fluid Dynamics (CFD) has gradually joined the wind tunnel and flight test as a primary flow analysis tool for aerodynamic designers. CFD has had its most favorable impact on the aerodynamic design of the high-speed cruise configuration of a transport. This success has raised expectations among aerodynamicists that the applicability of CFD can be extended to the full flight envelope. However, the complex nature of the flows and geometries involved places substantially increased demands on the solution methodology and resources required. Currently most simulations involve Reynolds-Averaged Navier-Stokes (RANS) codes although Large Eddy Simulation (LES) and Detached Eddy Suimulation (DES) codes are occasionally used for component analysis or theoretical studies. Despite simplified underlying assumptions, current RANS turbulence models have been spectacularly successful for analyzing attached, transonic flows. Whether or not these same models are applicable to complex flows with smooth surface separation is an open question. A prerequisite for answering this question is absolute confidence that the CFD codes employed reliably solve the continuous equations involved. Too often, failure to agree with experiment is mistakenly ascribed to the turbulence model rather than inadequate numerics. Grid convergence in three dimensions is rarely achieved. Even residual convergence on a given grid is often inadequate. This paper discusses issues involved in residual and especially grid convergence.

Key words: CFD, grid refinement, residual convergence, adjoint, turbulence model
AMS subject classification: 65N12, 65N22, 65N30, 65N50

Relationship between turbulence models and CFD grid

Thanks for listening

Please contact me:

donmcglinchey@outlook.com
d.mcglinchey@gcu.ac.uk
https://www.linkedin.com/in/donmcglinchey/

References

Che, H., Windows-Yule, K., O'Sullivan, C. and Seville, J. (2023) 'A novel semi-resolved CFD-DEM method with two-grid mapping: Methodology and verification', AIChE Journal, 69(11), e18321

Clarke, D.A., Sederman, A.J., Gladden, L.F. and Holland, D.J. (2018) 'Investigation of void fraction schemes for use with CFD-DEM simulations of fluidized beds', Industrial & Engineering Chemistry Research, 57(8), pp. 3002-3013

El Geitani, T. and Blais, B. (2023) 'Quadrature-centered averaging scheme for accurate and continuous void fraction calculation in computational fluid dynamics-discrete element method simulations', Industrial & Engineering Chemistry Research, 62(12), pp. 5394-5407

He, Y., Bayly, A.E., Hassanpour, A., Muller, F., Wu, K. and Yang, D. (2018) 'A GPU-based coupled SPH-DEM method for particle-fluid flow with free surfaces', Powder Technology, 338, pp. 548–562

Jiang, F., Liu, H., Chen, X. and Tsuji, T. (2022) 'A coupled LBM-DEM method for simulating the multiphase fluid-solid interaction problem', Journal of Computational Physics, 454, 110963

Kanitz, M. and Grabe, J. (2021) 'The influence of the void fraction on the particle migration: A coupled computational fluid dynamics–discrete element method study about drag force correlations', International Journal for Numerical and Analytical Methods in Geomechanics, 45(1), pp. 45–63

Li, X., Liu, G., Zhao, J., Yin, X. and Lu, H. (2022) 'IBM-LBM-DEM Study of Two-Particle Sedimentation: Drafting-Kissing-Tumbling and Effects of Particle Reynolds Number and Initial Positions of Particles', Energies, 15(9), 3297

Marchelli, F. and Di Felice, R. (2021) 'A Comparison of Ansys Fluent and MFiX in Performing CFD-DEM Simulations of a Spouted Bed', Fluids, 6(11), 382

Radl, S. and Municchi, F. (2015) Models on Heat and Mass Transfer, NanoSim Project Deliverable D4.3, Graz University of Technology (TUG)

Sun, R. and Xiao, H. (2018) 'Diffusion-Based Coarse Graining in Hybrid Continuum–Discrete Solvers: Theoretical Formulation and A Priori Tests', arXiv preprint, arXiv:1809.07008

References

Tsuji, K., Asai, M. and Kasama, K. (2023) 'Particle-Based Semi-Resolved Coupling Model for the Simulation of Internal Erosion in Soil Structures', in VIII International Conference on Particle-Based Methods (PARTICLES 2023)

Weerasekara, N., Potapov, A., Daroz, V., Bharadwaj, R. and Hanhiniemi, J. (2023) 'SPH-DEM techniques to solve complex flow structures in AG/SAG mills due to slurry and rock particle flows', White Paper/Technical Report

Wikipedia (2026) 'CFD-DEM', viewed 20 August 2026, https://en.wikipedia.org/wiki/CFD-DEM

Wikipedia (2026) 'Discrete element method', viewed 20 August 2026, https://en.wikipedia.org/wiki/Discrete_element_method

Wikipedia (2026) 'Smoothed-particle hydrodynamics', viewed 20 August 2026, https://en.wikipedia.org/wiki/Smoothed-particle_hydrodynamics

Wu, K., Yang, D. and Wright, N. (2016) 'A coupled SPH-DEM model for fluid-structure interaction problems with free-surface flow and structural failure', Computers and Structures, 177, pp. 141-161

Xia, T., Feng, Q., Wang, S., Zhang, J., Zhang, W. and Zhang, X. (2022) 'Numerical Study and Force Chain Network Analysis of Sand Production Process Using Coupled LBM-DEM', International Journal of Geo-Energy, 1(1)

Yang, G. C., Jing, L., Kwok, C. Y. and Sobral, Y. D. (2018) 'A comprehensive study of coupled LBM-DEM with immersed moving boundary', arXiv preprint, arXiv:1809.07008v1

Zakeri, A., Alizadeh Behjani, M. and Hassanpour, A. (2024) 'Fully Coupled CFD–DEM Simulation of Oil Well Hole Cleaning: Effect of Mud Hydrodynamics on Cuttings Transport', Processes, 12(4), 784

Zhu, S., Wu, C. and Yin, H. (2021) 'Virtual Experiments of Particle Mixing Process with the SPH-DEM Model', Materials, 14(9), 2199